A Photosensitizer Dinuclear Ruthenium Complex: Intramolecular Energy Transfer to a Covalently Linked Fullerene Acceptor

Dirk M. Guldi,*[a] Michele Maggini,*[b] Enzo Menna,[b] Gianfranco Scorrano,[b] Paola Ceroni,[c] Massimo Marcaccio,[c] Francesco Paolucci,*[c] and Sergio Roffia[c]

Dedicated to Professor Christopher Foote on the occasion of his 65th birthday

Abstract: A fullerene derivative (**5**) in which a dinuclear ruthenium complex is covalently linked to a fulleropyrrolidine (FP) through a rigid spacer has been prepared through azomethine ylide cycloaddition to C_{60}. Electrochemical and photophysical studies revealed that ground-state electronic interactions between the bimetallic ruthenium chromophore and the FP moiety are small. The absorption spectrum of **5** displays a metal-to-ligand charge transfer (MLCT) transition at about 620 nm in CH_2Cl_2 which is shifted by nearly 160 nm relative to that of a previously reported mononuclear dyad (**8**). The photophysical investigations have also shown that both in dichloromethane and acetonitrile the photoexcited MLCT state of dyad **5** transforms into the fullerene triplet excited state with a quantum yield of 0.19 and that, contrary to mononuclear dyad **8**, electron transfer, if any under the applied conditions, is negligible relative to energy transfer.

Keywords: dyads · energy transfer · fullerenes · ruthenium · sensitizers

Introduction

Molecules that combine several electro- and/or photoactive groups are of special interest as they can exhibit new properties arising from the interactions between the components. In particular, the synthesis and study of functionalized polypyridylruthenium(II) complexes with the electron-accepting fullerene core is particularly interesting as it may lead to new molecules with novel electron- (ET) or energy-transfer (ENT) features.[1] The importance of polypyridylruthenium complexes from both the electrochemical and photophysical point of view is longstanding.[2] Excitation of metal-to-ligand charge transfer (MLCT) transition generates the excited MLCT state, which displays attractive properties. Generally, this long-lived MLCT state has energetically high-lying levels that undergo efficient emission at room temperature in solution. This provides an excellent experimental probe for measuring the efficiency of intramolecular photoinduced ET or ENT processes in covalently linked donor–acceptor systems.[3] The functionalization of fullerenes, on the other hand, has given a strong impulse to the study of their interesting physicochemical characteristics, and a wide variety of derivatives[4] have been thoroughly investigated in light-driven ET or ENT reactions owing to the remarkable electron-acceptor properties of the fullerene sphere upon photoexcitation.[5, 6]

It has been shown, however, that the combination of more than one ruthenium center in a polymetallic array provides a greater flexibility in terms of excited-state donor energies, redox potentials and ground state absorption than their monometallic counterparts. This triggered an interdisciplinary interest to employ ruthenium complexes as building blocks in devices that perform light- and/or redox-induced functions.[7]

We report herein on the synthesis, electrochemistry and photophysical behavior of a bimetallic $[(bpy)_2Ru(dpq\text{-}FP)Ru(bpy)_2][PF_6]_4$ (bpy = 2,2′-bipyridine, dpq = 2,3-bipyridin-2-yl-quinoxaline, FP = fulleropyrrolidine) dyad in which the spacer between FP and dpq is an androstane skeleton. Photoinduced ENT from the metal complex to C_{60} occurs, and not ET, as previously observed for the corresponding monometallic $[Ru(bpy)_2(bpy\text{-}FP)][PF_6]_2$ dyad.[1d]

[a] Dr. Habil. D. M. Guldi
Radiation Laboratory, University of Notre Dame (USA)
E-mail: guldi.1@nd.edu

[b] Prof. M. Maggini, Dr. E. Menna, Prof. G. Scorrano
Centro Meccanismi CNR, Dipartimento di Chimica Organica Università di Padova
Via Marzolo 1, 35131 Padova (Italy)
Fax: (+39) 049-827-5662
E-mail: maggini@chor.unipd.it

[c] Prof. F. Paolucci, Dr. P. Ceroni, Dr. M. Marcaccio, Prof. S. Roffia
Dipartimento di Chimica "G. Ciamician"
Università di Bologna (Italy)
E-mail: paolucci@ciam.unibo.it

Results and Discussion

Synthesis: The synthetic strategy toward dyad **5** is outlined in Scheme 1. The route to **5** starts with readily available 2,3-dipyridin-2-yl-quinoxaline-6-carboxylic acid (**1**) (dpq-CO_2H) and requires three steps.

  0947-6539/01/0708-1597 $ 17.50+.50/0

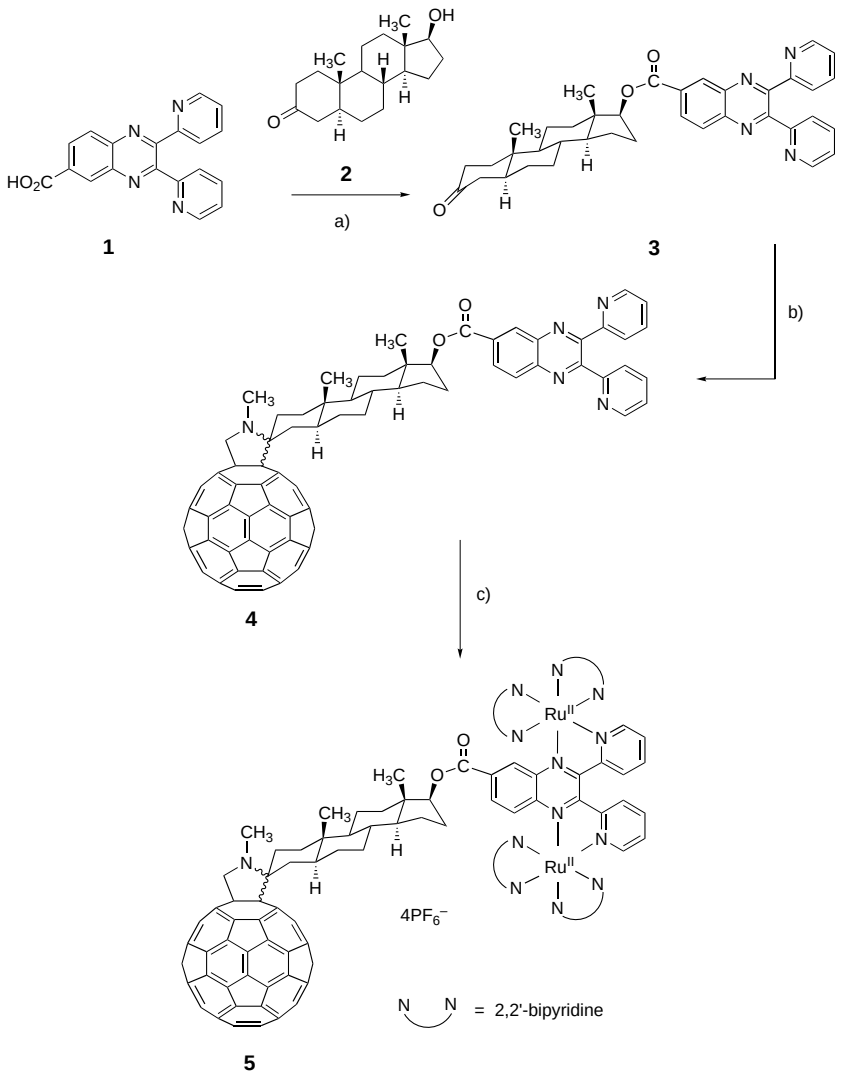

Scheme 1. Synthesis of dyad **5**. Reagents and conditions: a) DCC/DMAP, CH_2Cl_2, 24 h, 92%; b) *N*-methylglycine, C_{60}, toluene, reflux, 4 h, 32%; c) $Ru(bpy)_2Cl_2 \cdot 2H_2O$, NH_4PF_6, 1,2-dichloroethane, reflux, 4 h, 49%.

Esterification between **1** and commercially available androstane alcohol **2** (4,5-dihydrotestosterone) to afford ester–ketone **3** occurs in 92% yield under standard coupling conditions (dicyclohexylcarbodiimide/4-dimethylaminopyridine (DCC/DMAP)). Condensation of **3** with sarcosine in the presence of C_{60}[8] smoothly affords fulleropyrrolidine **4** in 32% yield (57% based on unreacted C_{60}) as a mixture of diastereoisomers. ^{1}H NMR spectroscopy and HPLC analysis revealed that **4** is in fact a mixture of two isomers in about 3:1 ratio. Bimetallic dyad **5** was synthesized by coordinating ligand **4** to ruthenium, through refluxing $[Ru(bpy)_2Cl_2] \cdot 2H_2O$ and **4** in 1,2-dichloroethane in the presence of excess NH_4PF_6 as previously reported for the preparation of dyad **8**.[1d]

The reaction was monitored by TLC (toluene/ethyl acetate 6:4), following the disappearance of **4**. The solution was evaporated to dryness and the residue dissolved in a minimum amount of CH_3CN, precipitated with a methanol/diethyl ether 1:1 mixture and carefully washed with CH_2Cl_2, MeOH and water to remove unreacted **4**, $[Ru(bpy)_2Cl_2]$ and excess NH_4PF_6 respectively. The desired dyad **5** was isolated in 49% yield as a green solid. Compound **5** is sparingly soluble in CH_3CN, acetone and chlorinated solvents but insoluble in toluene. ^{1}H and ^{13}C NMR spectra were not useful for the characterization of dyad **5**. The use of a diastereomeric mixture of ligand **4** produced dyad **5** as a mixture of isomers. As a consequence, mainly broad resonances in the aliphatic and aromatic regions were present in both the proton and carbon spectra of **5**. Dyad **5** was characterized by elemental analysis, mass spectrometry, optical spectroscopy, and electrochemical techniques (vide infra).

In our previous study regarding the mononuclear C_{60}–ruthenium dyad **8**,[1d] it was pointed out that the use of a diastereoisomeric mixture of ligands could, in principle, affect the photophysical characterization of the final C_{60}-based ruthenium dyad. In particular, the different spatial orientation of diastereoisomers may influence fundamental properties such as rate and extent of energy or electron transfer. After considerable experimentation, we found that the isomeric mixture of dyad **8** exhibits a similar behavior if compared to that of each diastereoisomer that was separately tested in photophysical experiments. We assumed that also the isomeric mixture of dyad **5** would perform similarly as that of each diastereoisomer. Therefore all the experiments described herein were carried out on the mixture of diastereoisomers of dyad **5**.

Derivatives **6** and **10** were synthesized and used as model compounds, together with fulleropyrrolidine **7**,[8] mononuclear dyad **8**,[1d] and metal complex **9**[1d] in the electrochemical and photophysical characterization of dyad **5**.

Electrochemistry: The analysis of the voltammetric behavior of dyad **5** has been based on that of models **6** and **7**, assuming no substantial interaction, in **5**, between the fullerene and the dinuclear ruthenium complex. The oxidation of **6** was investigated in CH_3CN. Two reversible, one-electron processes were recorded, and assigned to the two metal-centered $Ru^{II} \rightarrow Ru^{III}$ oxidations (Table 1).

The $E_{1/2}$ values (1.54 and 1.71 V) are comparable with those reported for a dinuclear ruthenium(II) complex containing an unsubstituted dpq ligand (1.47 and 1.62 V[7d]). The electron-

0947-6539/01/0708-1598 $ 17.50+.50/0 *Chem. Eur. J.* **2001**, *7*, No. 8

Table 1. $E_{1/2}$ (V vs. SCE) in THF/tetrabutylammonium hexafluorophosphate (TBAH) at 25 °C, unless otherwise noted. Working electrode: Pt

	Oxidations		Reductions								
			I	II	III	IV	V	VI	VII	VIII	IX
5	+1.52[a]	+1.70[a]	−0.23	−0.49	−0.89	−1.07	−1.41[c] −1.52[c]	−1.71	−1.83	−2.20	−2.73[b]
6	+1.54[a]	+1.71[a]	−0.23	−0.91	−1.41[c] −1.50	−1.81	−1.97	−2.26	−2.6[c] −2.7[c]		
7			−0.47	−1.05	−1.70	−2.16	−2.93				

[a] Acetonitrile solution. [b] Bielectronic process. [c] Obtained from digital simulation.

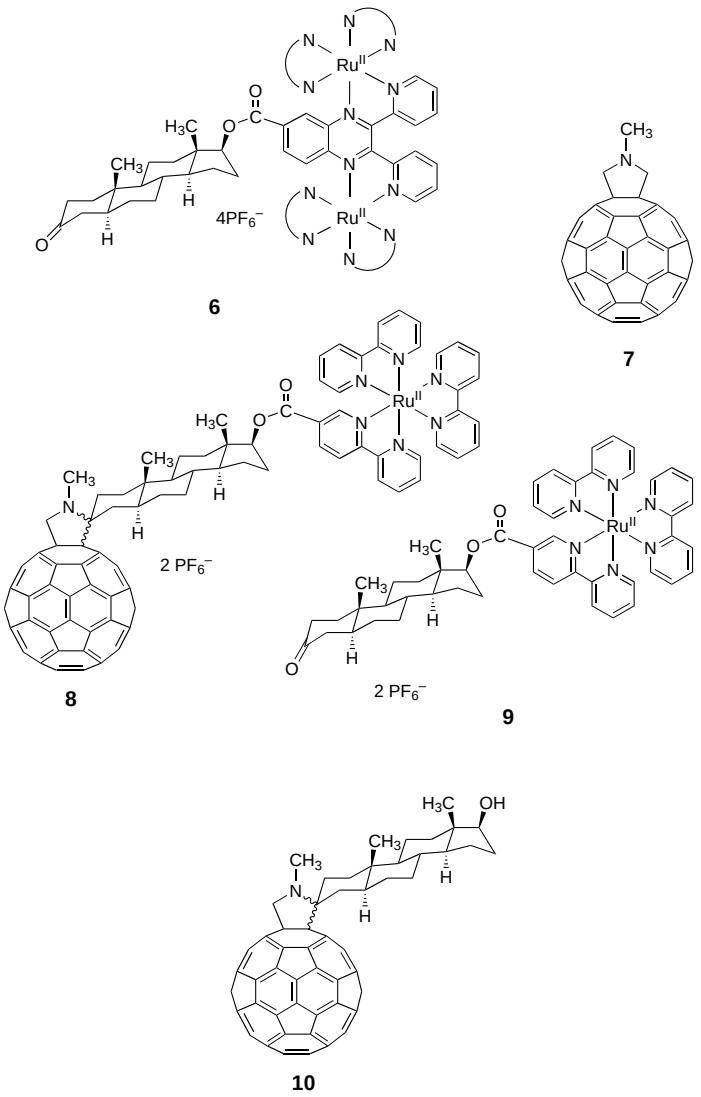

withdrawing effect of the ester substituent in the bridging ligand dpq is probably responsible of the small anodic shift in **6**, of both oxidations processes. Also, the 180 mV shift between them demonstrates that dpq allows a substantial interaction between the two metal centers. A similar splitting was already observed in other polynuclear complexes[7d, 9] and an explanation based on the superexchange theory has been given. Figure 1 displays the cyclic voltammogram of **6** in the cathodic region. Seven reduction peaks are shown and hereafter denoted by Roman numerals. Peaks I, II, IV, V, and VI correspond to reversible, one-electron reduction processes whose $E_{1/2}$ values could be directly measured

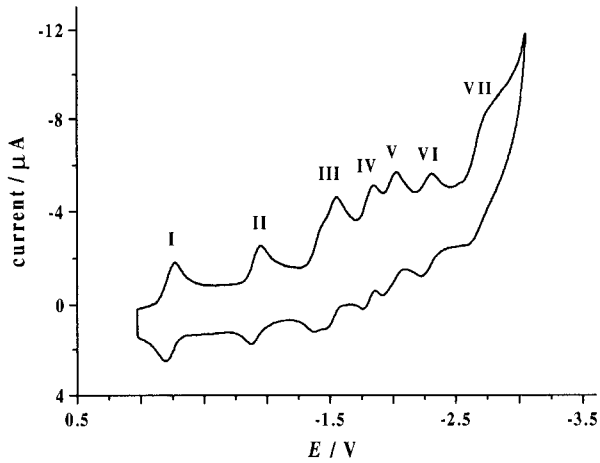

Figure 1. Cyclic voltammogram of **6** (0.5 mM) in THF (0.05 M TBAH). T = 25 °C, v = 0.5 V s^{-1}, working electrode: Pt.

(Table 1). Peak III results from the overlap of two reversible, one-electron reductions, whose $E_{1/2}$ value could be obtained only by digital simulation. The simulation also provided the $E_{1/2}$ values (Table 1) for the processes under peak VII, assuming an overall exchange of two electrons. The reversibility of the reduction processes under peak VII was difficult to establish owing to poor resolution.

By comparison with the electrochemical properties of similar ruthenium(II) complexes containing pyrazine ligands,[10] we propose the following assignment of the nine reduction processes of derivative **6**: 1) peaks I, II, and VI correspond to three successive reductions of the dpq bridging ligand; 2) peak IV, peak V, and the two nearly-overlapping processes comprised in peak III correspond to the one-electron reductions of the four bpy ligands, and 3) the two processes under peak VII are the second reduction of two bpy units. The second reduction of the other two bpy units is probably located outside the available potential window. In line with the above assignment, the splitting between the two processes under peak III and that between peaks IV and V is that expected for the interaction between equivalent bpy ligands in dinuclear complexes.[10] It is worth noting that the dpq-centered reductions are anodically shifted by about 150–200 mV relative to those reported for a dinuclear ruthenium(II) complex containing an unsubstituted dpq ligand.[7d] The electron-withdrawing effect of the ester substituent probably makes the dpq reductions easier. Neither reduction nor oxidation processes attributable to the androstanone moiety were observed, in agreement with our previously reported fullerene-based dyad **8**.[1d]

Fulleropyrrolidine **7** shows five reversible, one-electron reduction peaks[1d] whose $E_{1/2}$ values are reported, for the sake of comparison, in Table 1.

Figure 2a shows the cyclic voltammogram of dyad **5** in CH_3CN at 25 °C. In analogy to model **6**, the two reversible, one-electron peaks are the two metal-centered $Ru^{II} \rightarrow Ru^{III}$ oxidations whose $E_{1/2}$ values are reported in Table 1. In the cathodic region, significant complications arise from the

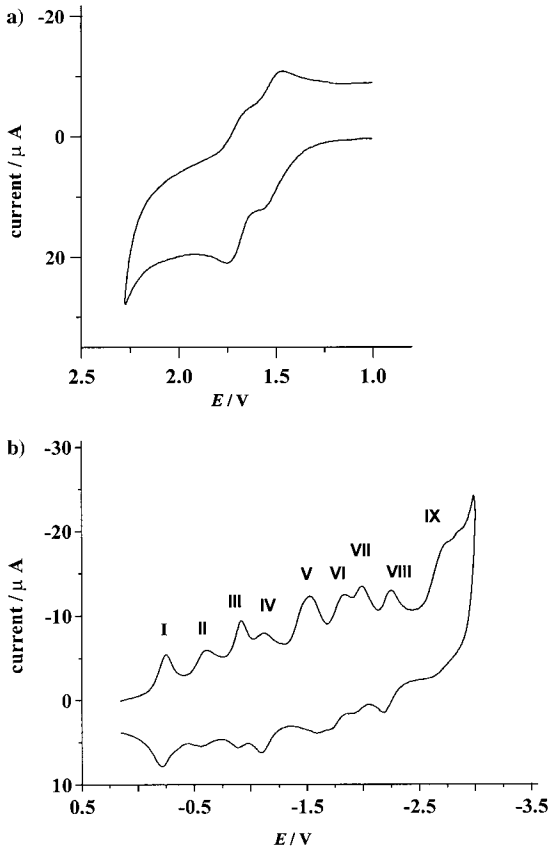

Figure 2. Cyclic voltammogram of **5**: a) 0.5 mM in CH_3CN (0.05 M TBAH); b) < 0.2 mM in THF (0.05 M TBAH). $T = 25$ °C, $v = 0.5$ V s^{-1}, working electrode: Pt.

adsorption of the dyad onto the electrode surface, which occurs in both CH_3CN and THF, at room temperature (see Figure 2b). Also the low solubility of **5** in THF, along with the chemical instability of the multiply reduced species, concurred to make the analysis of the cyclic voltammograms, and the calculation of the $E_{1/2}$ values for each redox process, rather difficult particularly at potentials beyond −2.5 V. However, the comparison of the CV pattern of **5** with that of models **6** and **7** allowed a reasonable assignment of the reduction processes. In contrast to mononuclear dyad **8**, it has been found that the first reduction of the dinuclear dyad is a ligand-centered (dpq) rather than a fullerene-centered process, being the first reduction of the fullerene moiety located 260 mV towards more negative potentials than the dpq-centered one.

Absorption spectra: The ground-state absorption spectrum of dyad **5** displays transitions that can be assigned to the $[(bpy)_2Ru(dpq)Ru(bpy)_2]^{4+}$ and FP moieties as shown in Figure 3 where the spectrum of **5** is plotted together with those of model derivatives **6** and **10** in CH_2Cl_2 (between 350–750 nm). All fullerene-centered diagnostic bands of FP **7**[4b] are observed in FP **10** that has been used as a FP model because of its higher solubility in CH_2Cl_2.

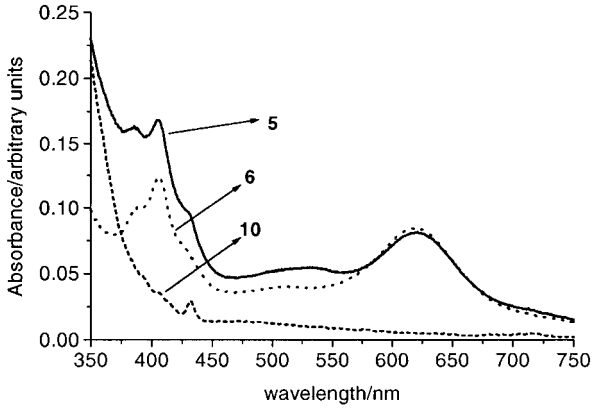

Figure 3. UV/Vis absorption spectra of dyad **5** (7.7×10^{-6} M) and reference derivatives **6** (7.1×10^{-6} M) and **10** (8.1×10^{-6} M) in CH_2Cl_2.

Dyad **5**, in CH_2Cl_2, reveals a MLCT transition at 620 nm which is red-shifted about 160 nm relative to that of the corresponding mononuclear dyad **8** in the same solvent.[1d] Interestingly, the MLCT absorption of **5** and **6** is also subjected to a red-shift relative to a previously reported dinuclear $[(bpy)_2Ru(dpq)Ru(bpy)_2]^{4+}$ complex whose MLCT transitions maximizes at 603 nm.[7d] This can be possibly rationalized in terms of the EW effect of the ester substituent in the bridging ligand dpq of dyad **5**.

In line with the results of the electrochemical study, no bands attributable to electronic interaction between fullerene and the ruthenium chromophores were observed.

Luminescence spectra: To investigate the extent of electronic interaction between the bimetallic ruthenium complex and the fullerene fragment in the excited state, emission measurements were carried out with dyad **5** in solvents of different polarity, and compared to that of model **6**. Equimolar solutions of **5** and **6** in CH_2Cl_2 show the same MLCT emission ($\lambda_{em}(max) = 710$ nm) at the 635 nm excitation wavelength. Interestingly, the luminescence yield in dyad **5** is subjected only to a moderate quenching (ca. 27%) relative to the emission of model **6**. This is in contrast to the behavior of mononuclear dyad **8** that, for instance in CH_2Cl_2, gives rise to a strong and effective quenching (89%) of the MLCT emission. Increasing the solvent polarity to CH_3CN (Figure 4) leads to a similar difference in MLCT luminescence between **5** and **6** (ca. 25%). This solvent independence may be considered as a first indication that ET represents probably a minor deactivation pathway for the MLCT excited state.

The low energy of the MLCT excited state of dyad **5** (1.75 eV vs. 1.97 eV[1d] for **8** in CH_3CN), which correlates with the early dpq-based reduction, makes the photoinduced intramolecular ET, from the excited binuclear ruthenium chromophore to the FP moiety, thermodynamically unfavored. The dielectric continuum model predicts in fact values

0947-6539/01/0708-1600 $ 17.50+.50/0 *Chem. Eur. J.* **2001**, *7*, No. 8

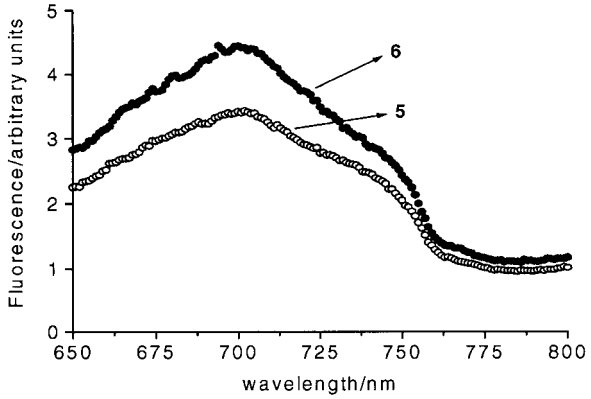

Figure 4. Emission spectra (excitation at 635 nm) of model **6** (●) and of dyad **5** (○) in CH_3CN at room temperature. All samples were studied under identical conditions and, therefore, the relative intensities represent relative emission quantum yields.

for the driving force ($-\Delta G_{ET}$) of the ET process of -0.17 and -0.34 eV[11] in CH_3CN and CH_2Cl_2, respectively, that is, ET is endoergonic in both media, thus corroborating the above conclusions based on the emission studies. For mononuclear dyad **8**, the same calculations gave a value of $+0.24$ eV in CH_3CN for the driving force indicating that ET is exergonic in that solvent.[1d]

Time-resolved photolysis: Although the conclusion of the emission studies infers that an intramolecular ET is unlikely to proceed, further examination of dyad **5** and models **6** and **10** by means of time-resolved transient absorption spectroscopy was carried out.

The differential absorption changes recorded upon excitation (532 nm, 18 ps) of model **6** are in large dictated by a transient bleaching of the MLCT ground-state transition in the region between 550 and 750 nm. By fitting the absorption-time profiles to a monoexponential decay, a lifetime of the photoexcited MLCT state of 30 ns was derived for **6** (Figure 5). This lifetime is substantially shorter than that measured for mononuclear ruthenium model **9**[1d] ($\tau = 180$ ns), but similar to that reported for the binuclear $[(bpy)_2Ru(dpq)Ru(bpy)_2]^{4+}$ complex ($\tau \sim 20$ ns).[7d] Intersystem crossing kinetics in polypyridylruthenium complexes take place on a sub-picosecond time base, from which we infer that the monitored transient characteristics (i.e., with a 18 ps time delay) are linked to the triplet MLCT states of mononuclear and binuclear ruthenium complexes.[12]

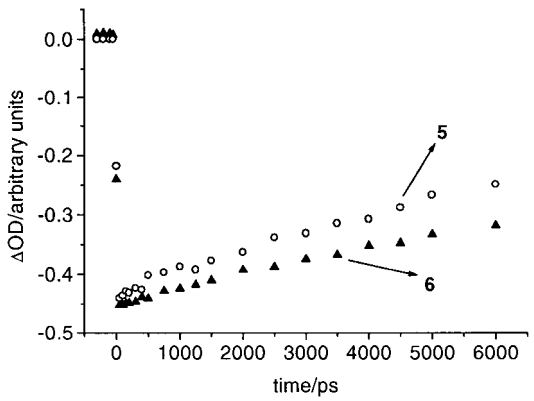

Figure 5. Time absorption profiles recorded at 660 nm for model **6** (▲) and dyad **5** (○) in CH_3CN at room temperature.

An extension of the monitored time-window to the nano-/microsecond regime helped to confirm the differential absorption changes developing during the picosecond experiments. Again, the displayed spectral region (Figure 6) is dominated by a strong bleaching originating from the d($\pi-\pi^*$) transitions of dpq and bpy in the visible region ($\sim$630 nm) and the ligand-based $\pi-\pi^*$ transitions in the UV region ($\sim$430 nm). The transient absorption changes, throughout the UV/Vis region, uniformly give rise to a lifetime of 30 ns for the MLCT state in **6**, whose decay leads to a quantitative recovery of the ground state.

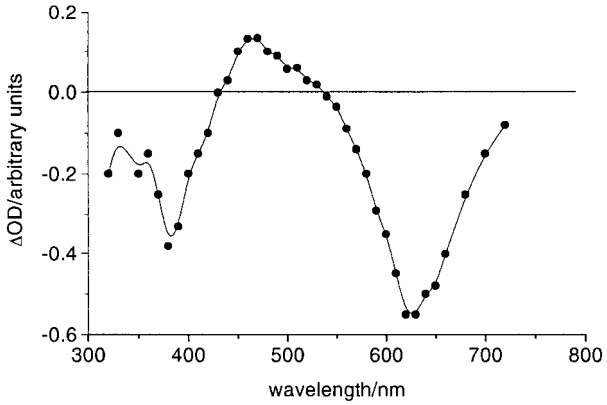

Figure 6. Differential absorption spectrum obtained upon flash photolysis of model **6** (2.0×10^{-6} M) in CH_3CN with a 8 ns laser pulse at 532 nm.

In the case of the fullerene model (i.e., either FP **7** or FP **10**) a strong absorption maximum was registered around 880 nm immediately after the laser excitation. This feature is a known fingerprint of the FP singlet excited state absorption, which decays in the 900 nm region rapidly with a lifetime of 1.8 ns. A concomitant grow-in of a new transient absorption, disclosing a doublet of maxima at 360 and 690 nm, relates to the intersystem crossing (ISC) to the FP triplet excited state. In oxygen-free solutions, a clean monoexponential recovery of the singlet ground-state follows at low FP concentration and low laser power, affording a triplet lifetime of nearly 50 μs under our conditions. Compared to the dinuclear ruthenium model **6** no bleaching was observed for FP throughout the entire visible region.

In analogy to the excitation of model **6**, irradiation of dyad **5** with 532 nm laser pulses gave the MLCT excited state of the dinuclear ruthenium chromophore (90.6%). In the picosecond-resolved experiments the differential bleaching between 550 and 750 nm, recorded after an 18 ps laser pulse (Figure 5 and Figure 7), is a qualitative match to that noted for model **6**. Importantly, a slightly shorter lifetime (22 ns) was measured with respect to **6**.

To confirm the MLCT excited state formation and to probe the MLCT excited state deactivation, the picosecond measurements were complemented by nanosecond experiments. Differential absorption changes in the UV/Vis range recorded immediately after photolyzing dyad **5** in oxygen-free CH_3CN,

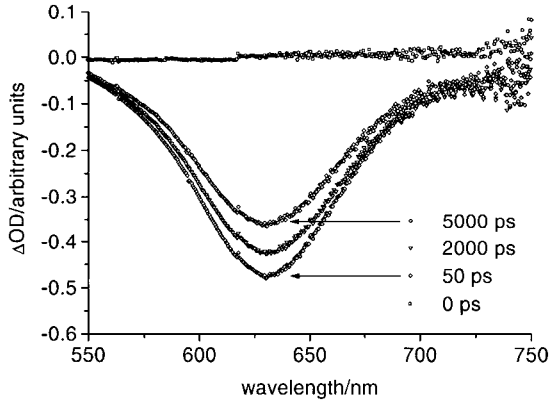

Figure 7. Time-resolved difference absorption spectra of dyad **5** (2.0×10^{-6} M) in CH_3CN 0, 50, 2000 and 5000 ps after excitation with a 18 ps laser pulse at 532 nm.

are plotted in Figure 8 ((●); 50 ns after the laser pulse). The light-induced formation of the transient bleaching reveals a series of minima at 310, 410, and 630 nm. These spectral characteristics are not only reminiscent to those reported for the photoexcited ruthenium complex **6** but are also identical to those observed during the course of the picosecond experiments.

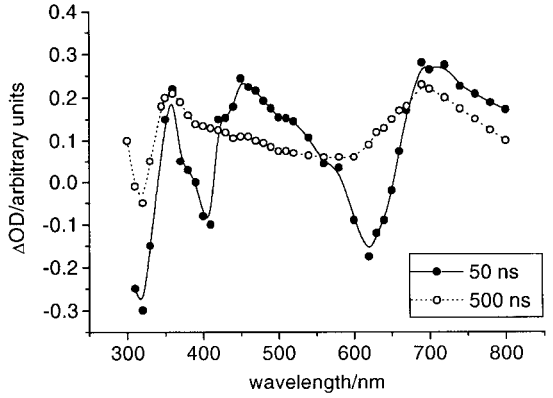

Figure 8. Differential absorption spectrum obtained 50 ns (●) and 500 ns (○) upon flash photolysis of dyad **5** (2.0×10^{-6} M) in CH_3CN with a 8 ns laser pulse at 532 nm.

A detailed kinetic analysis of the time-absorption profiles show that the spectral features of the MLCT excited state transform slowly into a new species (Figure 8 (○); 500 ns after the laser pulse). Importantly, this conversion process is characterized by both growth (≈630 nm) and decay dynamics (≈450 nm), depending on the relative absorbances of the precursor state and the newly formed product. The strongly absorbing photoproduct displays a set of two maxima at 360 and 690 nm, respectively. These features agree well with those of the triplet-excited state of FP **10**. In addition, the recorded lifetime of 43 μs, similar to that observed when FP **10** is directly excited, suggests an intramolecular energy transfer to the fullerene-excited triplet state.

Interestingly, the acceleration of the MLCT excited state decay of **5** relative to model **6** (i.e., 22 ns vs. 30 ns) resembles the overall luminescence quenching (see above; ca. 27%).

Pulse radiolysis: As a specific and final test to confirm the energy transfer rather than the electron transfer mechanism, models **6** and **10** were oxidized and reduced, respectively, in a set of complementary radiolytic experiments.[13, 14] It was deemed important to simulate the spectral characteristics of the charge-separated radical pair and to compare them to those noted following the excitation of dyad **5** (i.e., during the pico- and nanosecond regimes). In fact, both the UV/Vis and NIR regions, displaying characteristic fingerprints for an oxidized ruthenium complex (Figure 9) or a fullerene π-radical anion, lack clear evidence that would suggest the formation of a charge-separated radical pair.

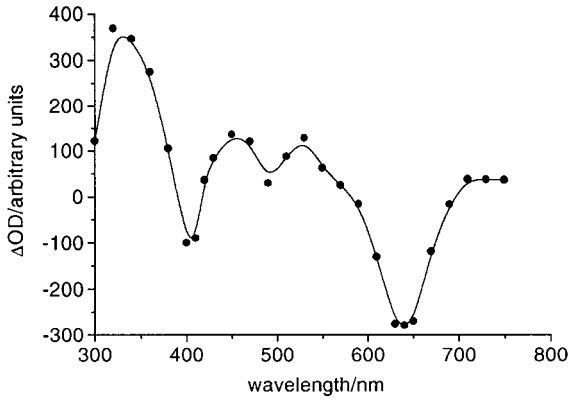

Figure 9. Radiolytic oxidation of model **6**: transient absorption spectrum of ruthenium(III) obtained upon pulse radiolysis in N_2O-saturated aqueous solution containing 0.1 M HCl.

Quantum yield determination: In addition to the transient absorption changes, the quantum yield of the fullerene triplet excited state (ε at 710 nm = 14000 $M^{-1}cm^{-1}$) in dyad **5** was determined using the comparative method in reference to a known standard, namely pristine C_{60} ($\Phi_T \approx 1$, ε at 750 nm = 20200 $M^{-1}cm^{-1}$).[15] Measurements in deoxygenated CH_2Cl_2 solutions gave rise to a quantum yield $\Phi = 0.19$, after subtracting the fullerene ground state absorption at 532 nm (i.e., 9.4% fullerene and 90.6% dinuclear ruthenium(II) moiety). This corroborates the transient absorption changes and documents the generation of the fullerene triplet excited state in **5** by photoexcitation of the ruthenium chromophore, followed by an intramolecular triplet–triplet energy transfer process evolving from the MLCT excited state of the dinuclear ruthenium complex.

In the context of energy transfer in fullerene-based materials, a series of oligo(naphthylenevinylene)–fullerene and perylene–fullerene assemblies should be mentioned, in which both singlet–singlet energy transfer and intramolecular electron transfer were found to take place and, more importantly, to compete with each other.[16] However, a number of fundamental differences should be pointed out, which have significant effects on the mechanism, rates, and efficiencies. In these systems, a direct link of the photosensitizer to the fullerene provides the grounds for a strong coupling between the donor and acceptor moieties and, subsequently, for very fast and efficient transfers. Besides the different linkages, the lack of spin-orbit coupling in the oligo(naphthylenevinylene) and perylene photosensitizers is

0947-6539/01/0708-1602 $ 17.50+.50/0 *Chem. Eur. J.* **2001**, *7*, No. 8

another meaningful factor in determining the origin of the excited state energy. Finally, the mechanism, that is, singlet–singlet versus triplet–triplet exchange should be considered.

Formation of singlet oxygen: To probe the reactivity of the product arising from photoexcitation of dyad **5**, the bimolecular quenching rate constant with molecular oxygen was measured in CH_2Cl_2 solutions purged with variable amounts of O_2. The determined rate constant (1.5×10^9 M^{-1} s^{-1}) is very similar to those noted for pristine fullerene and *N*-methylfulleropyrrolidines.[15] This suggests that dyad **5** generates, similar to other fullerenes, singlet oxygen through the energy transfer route.

Conclusion

A fulleropyrrolidine covalently linked to a 2,3-bipyridin-2-ylquinoxaline ligand was incorporated into a novel dinuclear ruthenium(II)-based dyad. Both electrochemical and photophysical studies have shown that the fullerene and dinuclear ruthenium complex in the dyad interact only weakly in the ground state. The photophysical characterization revealed that intramolecular energy transfer from the ruthenium MLCT excited state (1.75 eV) to the functionalized fullerene takes place with a quantum yield of 0.19 and that ET, if any, represents probably a minor deactivation pathway for the MLCT excited state. Our current efforts are directed to the development of photovoltaic devices containing donor–acceptor systems such as dyad **5**, using layer-by-layer deposition techniques.[17]

Experimental Section

General: Details regarding the instrumentation used in this work to characterize compounds **1**, **3**–**6**, and **10** have been described elsewhere.[18] Absorption spectra were recorded with a Milton Roy Spectronic 3000 Array spectrophotometer. Emission spectra were recorded on a SLM 8100 Spectrofluorimeter. Fluorescence spectra were measured in CH_2Cl_2 (5.0×10^{-5} M) at liquid nitrogen or room temperature. A 570 nm long-pass filter in the emission path was used to eliminate the interference from the solvent and stray light. Long integration times (20 s) and low increments (0.1 nm) were applied. The slits were 2 and 8 nm. Each spectrum was an average of at least five individual scans.

Electrochemical instrumentation and measurements: The one-compartment electrochemical cell was of air-tight design with high-vacuum glass stopcocks fitted with either Teflon or Kalrez (DuPont) O-rings to prevent contamination by grease. The connections of the high-vacuum line and Schlenck apparati used for solvents were spherical joints also fitted with Kalrez O-rings. The pressure in the electrochemical cell prior to performing the trap-to-trap distillation of the solvent was typically $1.0-2.0 \times 10^{-5}$ mbar. The working electrode consisted either of a 0.6 mm-diameter platinum wire (0.15 cm^2 approximately) sealed in glass or in a Pt disc ultramicroelectrode ($r = 5$ μm), also sealed in glass. The counter electrode consisted of a platinum spiral and the quasi-reference electrode was a silver spiral. The quasi-reference electrode drift was negligible for the time required by a single experiment. Both the counter and the reference electrode were separated from the working electrode by ≈0.5 cm. Potentials were measured with the ferrocene standard and are always referenced to the saturated calomel electrode (SCE). $E_{1/2}$ values correspond to $(E_{pc} + E_{pa})/2$ from cyclic voltammetry. In some experiments a SCE reference electrode was used, separated from the working electrode compartment by a sintered glass frit. Ferrocene was used as an internal standard for confirming the electrochemical reversibility of a redox couple. Voltammograms were recorded with a AMEL Model 552 potentiostat or a custom made fast potentiostat controlled by either a AMEL Model 568 function generator or a ELCHEMA Model FG-206 F. The data acquisition was performed with a Nicolet Model 3091 digital oscilloscope interfaced to a PC. Temperature control was accomplished within 0.1 °C with a Lauda Klein-Kryomat thermostat. The DigiSim 2.1 software by Bioanalytical Systems Inc., or the Antigona software developed by Dr. Loic Mottier (http://www.ciam.unibo.it/electrochem.html) was used for the simulation of the CV curves.

Flash-photolysis and pulse-radiolysis instrumentation and measurements: Picosecond laser flash photolysis experiments were carried out with 532 nm laser pulses from a mode-locked, Q-switched Quantel YG-501 DP Nd:YAG laser system (pulse width 18 ps) and corresponding nanosecond laser flash photolysis with laser pulses from a Qunta-Ray CDR Nd:YAG system (532 nm, 6 ns pulse width) or alternatively from a Molectron UV-400 nitrogen laser system (337.1 nm, 8 ns pulse width).[19] Pulse radiolysis experiments were performed by utilizing 50 ns pulses of 8 MeV electrons from a Model TB-8/16-1S Electron Linear Accelerator.[20]

Materials: C_{60} was purchased from Bucky USA (99.5 %). All other reagents were used as purchased from Aldrich. *cis*-Bis(2,2′-bipyridine-N,N′)-dichlororuthenium(II) dihydrate,[21] *N*-methylfulleropyrrolidine **7**,[8] mononuclear dyad **8** $[Ru(bpy)_2(L1)][PF_6]_2$ (L1 = *N*-methylfulleropyrrolidine-2-spiro-17′β-(ol-2,2′-bipyridylcarboxylate)-5′α-androstanyl),[1d] mononuclear ruthenium(II) model **9** $[Ru(bpy)_2(L2)][PF_6]_2$ (L2 = 17β-(ol-2,2′-bipyridylcarboxylate)-5α-androstan-3-one),[1d] were prepared as described in the literature. All solvents were distilled prior to use. Dichloromethane and acetonitrile employed for UV/Vis, steady-state luminescence, pico- and nanosecond flash photolysis and pulse radiolysis measurements were commercial spectrophotometric grade solvents that were carefully deoxygenated prior to use. TBAH (puriss. from FLUKA) was used as supporting electrolyte as received. THF (LiChrosolv, Merck) was treated according to a procedure reported elsewhere.[22] For the electrochemical experiments, THF was distilled into the electrochemical cell, prior to use, using a trap-to-trap procedure.

Synthesis of $[Ru_2(bpy)_4(4)][PF_6]_4$ (5): A solution of fulleropyrrolidine **4** (24 mg, 0.018 mmol), $[Ru(bpy)_2Cl_2] \cdot 2H_2O$ (31 mg, 0.060 mmol) and NH_4PF_6 (53 mg, 0.32 mmol) in 1,2-dichloroethane (7 mL) was heated to reflux for 4 h under a nitrogen atmosphere in the dark. The reaction was monitored by TLC (toluene/AcOEt 6:4), following the consumption of **4**. After filtration, the solvent was evaporated under reduced pressure and the residue dissolved in a minimum amount of CH_3CN, followed by precipitation by MeOH/Et_2O (1:1). The precipitate, isolated by centrifugation, was washed with CH_2Cl_2, MeOH, water, and then dried in vacuum affording **1** (24.5 mg, 49 %) as a green solid. NMR (CD_3CN, 25 °C): proton and carbon NMR spectra show mainly broad resonances in the aliphatic and aromatic regions (see text); IR (KBr): $\tilde{\nu} = 2925$, 1718, 1447, 841, 764, 558, 528 cm^{-1}; UV/Vis (CH_2Cl_2): λ_{max} (ε) = 250 (98 600), 279 (111 000), 382 (19 800), 405 (22 000), 620 nm (10 600 mol^{-1} dm^3 cm^{-1}); MS (MALDI): *m/z* (%): 2174 $[M - 4PF_6]^+$; MS (FAB) 1762 $[M - 4PF_6(bpy)_2Ru]^+$, 720 $[C_{60}]^+$; elemental analysis calcd (%) for $C_{140}H_{77}N_{13}O_2F_{24}P_4Ru_2$ (2755.2): C 61.0, H 2.8, N 6.6; found: C 58.7, H 2.8, N 6.1.

***N*-methylfulleropyrrolidine-2-spiro-17′β-(ol-2,3-bipyridin-2-yl-quinoxaline-6-carboxylate)-5′α-androstanyl (4)**: A solution of C_{60} (140 mg, 0.19 mmol), sarcosine (81 mg, 0.91 mmol), and ester–ketone **3** (130 mg, 0.22 mmol) in toluene (140 mL) was heated to reflux for 4 h. The reaction was monitored by TLC (toluene/AcOEt 6:4), following the formation of **4** ($R_f = 0.63$). The solvent was evaporated under reduced pressure, and the crude product purified by flash column chromatography (SiO_2). Elution with toluene and subsequently with toluene/AcOEt 9:1 gave **4** (81 mg, 32 %) along with unreacted C_{60} (80 mg, 57 %). ^{1}H NMR (250 MHz, CD_2Cl_2/CS_2 2:1, 25 °C, TMS): fulleropyrrolidine **4** is a mixture of diastereoisomers (see text). The resonances relative to the minor diastereoisomer are given only when possible: $\delta = 8.77$ (d, ^4J(H,H) = 1.4 Hz, 1H), 8.73 (minor, d, ^4J(H,H) = 1.5 Hz, 1H), 8.32 (dd, ^3J(H,H) = 8.8 Hz, ^4J(H,H) = 1.9 Hz, 1H), 8.28 (minor, dd, ^3J(H,H) = 8.8 Hz, ^4J(H,H) = 1.5 Hz, 1H), 8.10–8.19 (m, 3H), 7.97–8.02 (m, 2H), 7.75–7.82 (m, 2H), 7.14–7.20 (m, 2H), 4.95 (m, 2H; pyrrolidine-CH_2), 4.92 (t, ^3J(H,H) = 7.8 Hz, 1H; CH at position 17 of the androstane), 4.79 (minor, t, ^3J(H,H) = 7.8 Hz; CH at position 17 of the androstane), 4.54 (minor, s, 2H; pyrrolidine-CH_2), 3.46 (s, 3H; N–CH_3), 2.88 (minor, s, 3H; N–CH_3), 1.04 (minor, s, 3H; CH_3), 1.02 (s, 3H; CH_3),

0.98 (s, 3H; CH_3). Resonances due to the androstane moiety, that appear as a complex cluster of signals between $\delta = 0.5$ and 2.8, are not reported); ^{13}C NMR (62.9 MHz, CD_2Cl_2/CS_2 2:1, 25 °C, TMS): $\delta = 165.23$, 165.11, 157.48, 157.45, 155.85, 154.06, 153.51, 148.17, 146.90, 146.53, 146.40, 146.32, 146.09, 145.98, 145.88, 145.57, 145.39, 145.30, 145.21, 145.17, 145.07, 144.63, 144.48, 143.32, 142.98, 142.85, 142.79, 142.69, 142.50, 142.46, 142.40, 142.30, 142.22, 142.08, 141.96, 141.92, 141.88, 140.36, 140.31, 140.05, 140.00, 136.36, 135.56, 135.49, 135.42, 132.42, 131.757, 129.94, 129.60, 124.07, 123.97, 123.12, 123.03, 84.18, 84.12, 80.10, 78.88, 76.46, 72.26, 69.69, 69.63, 65.31,.54.89, 54.80, 51.29, 50.88, 43.45, 43.26, 42.62, 38.87, 37.57, 37.30, 36.67, 36.18, 36.05, 35.92, 35.68, 35.62, 33.90, 32.21, 31.96, 29.11, 28.20, 27.39, 24.11, 21.11, 12.67, 12.55, 12.32; IR (KBr): $\tilde{\nu} = 2924$, 1721, 1270, 1246, 1094, 787, 762, 528 cm^{-1}; UV/Vis (CH_2Cl_2): λ_{max} (ε) = 254 (132 000), 318 (50 700), 432 nm (3400 $mol^{-1} dm^3 cm^{-1}$); MS (MALDI): *m/z* (%): 1347 $[M]^+$, 627 $[M - C_{60}]^+$; calcd exact mass (HR-FAB, 3-nitrobenzyl alcohol (3-NBA)/Gly/1% trifluoroacetic acid (TFA) as matrix): 1348.3652; found 1348.3647 (−0.3 ppm); elemental analysis calcd (%) for $C_{100}H_{45}N_5O_2$ (1348.5): C 89.0, H 3.4, N 5.2; found C 88.9, H 3.1, N 5.2.

17β-(ol-2,3-bipyridin-2-yl-quinoxaline-6-carboxylate)-5α-androstan-3-one (3): A mixture of dpq-CO_2H **1** (164 mg, 0.48 mmol), DMAP (35 mg, 0.29 mmol), and DCC (122 mg, 0.59 mmol) in CH_2Cl_2 (3 mL) was stirred at room temperature for 20 min. A solution of 4,5-dihydroxytestosterone **2** (168 mg, 0.58 mmol) in CH_2Cl_2 (2 mL) was added and the mixture was stirred for 24 h at room temperature. The reaction was monitored by TLC (toluene/AcOEt 1:1), following the formation of **3** ($R_f = 0.64$). The solvent was evaporated under reduced pressure and the crude product purified by flash column chromatography (SiO_2, eluent toluene/AcOEt 65:35) affording **6** (266 mg, 92%) as a white solid. An analytical sample was obtained by crystallization from isopropanol: m.p. 252–254 °C; ^1H NMR (250 MHz, $CDCl_3$, 25 °C, TMS): $\delta = 8.99$ (d, ^4J(H,H) = 1.46 Hz, 1H), 8.48 (m, 3H), 8.34 (d, ^3J(H,H) = 8.79 Hz, 1H), 8.10 (t, ^3J(H,H) = 7.81 Hz, 2H), 7.93 (m, 2H), 7.35 (m, 2H), 5.02 (m, 1H), 2.6–0.8 (unresolved), 1.12 (s, 3H), 1.10 (s, 3H); ^{13}C NMR (62.9 MHz, $CDCl_3$, 25 °C, TMS): $\delta = 211.84$, 165.58, 156.88, 156.80, 153.82, 153.26, 148.49, 143.04, 140.34, 136.92, 136.84, 132.33, 131.68, 130.16, 129.55, 124.35, 124.25, 123.35, 123.24, 83.98, 53.70, 50.61, 46.59, 44.62, 43.14, 38.46, 38.08, 36.94, 35.70, 35.19, 33.89, 31.21, 28.73, 27.71, 24.89, 23.65, 20.90, 12.48, 11.46; IR (KBr): $\tilde{\nu} = 2932$, 1718, 1273, 1099, 790 cm^{-1}; elemental analysis calcd (%) for $C_{38}H_{40}N_4O_3$ (600.8): C 76.0, H 6.7, N 9.3; found: C 75.8, H 6.7, N 9.2.

[Ru_2(bpy)$_4$(17β-(ol-2,3-bipyridin-2-yl-quinoxaline-6-carboxylate)-5α-androstan-3-one)][PF_6]$_4$ (6): A solution of **3** (86 mg, 0.14 mmol), [Ru(bpy)$_2$-Cl_2]·2H_2O (144 mg, 0.28 mmol) and NH_4PF_6 (155 mg, 0.95 mmol) in 1,2-dichloroethane (12 mL) was heated to reflux for 24 h under a nitrogen atmosphere in the dark. The reaction was monitored by TLC (brine/acetone/MeOH 6:2:2), following the formation of **6** ($R_f = 0.17$). The solvent was evaporated under reduced pressure and the residue, dissolved in a minimum amount of acetone, precipitated by addition of Et_2O. The precipitate, isolated by centrifugation, was washed with a 1:1 acetone/Et_2O solvent mixture, and then CH_2Cl_2, and then dried under vacuum affording **6** (206 mg, 73%) as a green solid. NMR (CD_3CN, 25 °C, TMS): the proton and carbon NMR spectra show a complex and unresolved host of resonances in the aliphatic and aromatic regions. Derivative **6** is in fact a mixture of diastereoisomers and its NMR behavior is similar to that discussed for dyad **5** (see text); IR (KBr): $\tilde{\nu} = 2929$, 1709, 1448, 840, 764, 558 cm^{-1}; UV/Vis (CH_2Cl_2): $\lambda_{max} = (\varepsilon)$ 286 (71 000), 389 (14 500), 405 (17 400), 620 nm (11 900 $mol^{-1} dm^3 cm^{-1}$); MS (MALDI): *m/z* (%): 1718 $[M - 2PF_6]^+$; elemental analysis calcd (%) for $C_{78}H_{72}N_{12}O_3F_{24}P_4Ru_2$ (2007.5): C 46.7, H 3.6, N 8.4; found: C 47.0, H 3.6, N 8.5.

2,3-Dipyridin-2-yl-quinoxaline-6-carboxylic acid (1): A solution of 2,2′-bipyridine (2.03 g, 9.6 mmol) and 3,4-diaminobenzoic acid (1.49 g, 10.6 mmol) in ethanol (50 mL) was heated to reflux for 1.5 h. The formation of a gray precipitate was observed. The solid was filtered and crystallized from ethanol to afford **1** (2.41 g, 73%) as a gray solid: m.p. 232–235 °C; ^1H NMR (200 MHz, [D_6]DMSO, 25 °C, TMS): $\delta = 13.56$ (br s, 1H), 8.70 (s, 1H), 8.29 (m, 4H), 7.99 (m, 4H), 7.36 (t, 2H); ^{13}C NMR (62.9 MHz, [D_6]DMSO, 25 °C, TMS) $\delta = 166.69$, 156.76, 154.10, 153.53, 148.34, 142.32, 139.74, 137.15, 132.90, 130.97, 130.34, 129.65, 124.20, 124.14, 123.76, 123.68; IR (KBr): $\tilde{\nu} =$ 1689, 1587, 1354, 1312, 1271, 787 cm^{-1}; elemental analysis calcd (%) for $C_{19}H_{12}N_4O_2$ (328.3): C 69.5, H 3.7, N 17.0; found: C 69.6, H 3.5, N 17.0.

***N*-methyl-3,4-fulleropyrrolidine-2-spiro-5′α-androstanyl (10)**: A solution of C_{60} (53 mg, 0.074 mmol), sarcosine (19.2 mg, 0.22 mmol), and 4,5-dihydrotestosterone **2** (61.6 mg, 0.22 mmol) in toluene (50 mL) was heated to reflux for 3 h. The reaction was monitored by TLC (toluene/ethyl acetate 1:1) following the formation of **10** ($R_f = 0.67$). The crude product was purified by flash column chromatography (SiO_2, eluent toluene then toluene/AcOEt 9:1) affording 29.5 mg (38%) of **10** and 22.5 mg (42%) of unreacted C_{60}. ^1H NMR (250 MHz, CS_2/CD_2Cl_2 2:1, 25 °C, TMS): resonances relative to the major diastereoisomer are reported along with those of the minor one when detectable: $\delta = 4.96$ (m, 2H; pyrrolidine-CH_2), 4.54 (minor, s, 2H; pyrrolidine-CH_2), 3.59 (t, ^3J(H,H) = 8.30 Hz, 1H; CH at position 17 of the androstane), 3.46 (s, 3H; N−CH_2), 2.88 (minor, s, 3H; N-CH_2), 1.02 (minor, s, 3H; CH_2), 0.96 (s, 3H; CH_2), 0.71 (s, 3H; CH_2), 0.67 (minor, s, 3H; CH_2). Resonances due to the androstane moiety, that appear as a complex cluster of signals between $\delta = 0.5$ and 2.8, are not reported; ^{13}C NMR (62.9 MHz, CS_2/CD_2Cl_2 2:1, 25 °C, TMS): $\delta = 157.27$, 156.96, 156.82, 156.76, 156.11, 155.85, 155.13, 155.05, 146.89, 146.51, 146.40, 146.30, 146.08, 145.88, 145.56, 145.35, 145.19, 145.06, 144.48, 143.31, 142.69, 142.42, 142.29, 142.22, 141.97, 140.32, 140.03, 139.20, 135.54, 129.12, 128.35, 125.44, 84.17, 82.01, 81.92, 78.88, 76.44, 72.28, 69.67, 65.29, 55.04, 51.50, 51.12, 43.49, 43.30, 43.10, 42.66, 38.86, 37.25, 36.99, 36.69, 36.19, 36.03, 35.89, 33.89, 32.22, 31.99, 31.02, 30.90, 30.14, 25.18, 23.84, 23.74, 21.56, 21.14, 12.55, 12.32, 11.30, 11.23; IR (KBr): $\tilde{\nu} = 3435$, 2925, 2866, 2849, 1452, 528 cm^{-1}; UV/Vis (CH_2Cl_2): $\lambda_{max} = (\varepsilon)$ 238 (77 663), 300 (36 106), 430 nm (3500 $mol^{-1} dm^3 cm^{-1}$); MS (MALDI): *m/z* 1039 $[M+H]^+$; elemental analysis calcd (%) for $C_{81}H_{35}NO$ (1038.2): C 93.7, H 3.4, N 1.4; found: C 92.9, H 3.2, N 1.3; calcd exact mass (HR-FAB, 3-NBA/Gly/1%TFA as matrix): 1038.2797; found 1038.2774 (−2.2 ppm).

Acknowledgement

We thank Dr. R. Seraglia (CNR-Padova) for MALDI-MS data. Exact mass data were provided by the Washington University Mass Spectrometry Resource, an NIH Research Resource (Grant No. P41RR00954). We are indebted to Dr. S. Mondini for her contribution in working out detailed synthetic procedures. This work was in part supported by the Office of Basic Energy Sciences of the Department of Energy, by CNR through CMRO (legge 95/95), by MURST (contracts No. 9803194198 and No. 9803104402), and by the University of Bologna (Funds for Selected Research Topics). This is document NDRL-4255 from the Notre Dame Radiation Laboratory. M.M. and D.G. thank NATO for a travel grant (Grant No. CRG960099).

[1] a) D. M. Guldi, M. Maggini, S. Mondini, F. Guerin, J. H. Fendler, *Langmuir* **2000**, *16*, 1311; b) A. Polese, S. Mondini, A. Bianco, C. Toniolo, G. Scorrano, D. M. Guldi, M. Maggini, *J. Am. Chem. Soc.* **1999**, *121*, 3456; c) D. Armspach, E. C. Constable, F. Diederich, C. E. Housecroft, J.-F. Nierengarten, *Chem. Eur. J.* **1998**, *4*, 723; d) M. Maggini, D. M. Guldi, S. Mondini, G. Scorrano, F. Paolucci, P. Ceroni, S. Roffia, *Chem. Eur. J.* **1998**, *4*, 1992; e) D. Armspach, E. C. Constable, F. Diederich, C. E. Housecraft, J.-F. Nierengarten, *J. Chem. Soc. Chem. Commun.* **1996**, 2009; f) N. S. Sariciftci, F. Wudl, A. J. Heeger, M. Maggini, G. Scorrano, M. Prato, J. Bourassa, P. C. Ford, *Chem. Phys. Lett.* **1995**, *247*, 210; g) M. Maggini, A. Donò, G. Scorrano, M. Prato, *J. Chem. Soc. Chem. Commun.* **1995**, 845.

[2] a) *Photochemistry and Photophysics of Coordination Compounds* (Eds.: H. Yersin, A. Vogler), Springer, Berlin, **1987**; b) *Photochemistry of Polypyridine and Porphyrin Complexes* (Ed.: K. Kalyanasundaram, K.), Academic Press, London, **1991**; c) *Charge Transfer Photochemistry* (Eds.: O. Horvath, K. L. Stevenson), VCH, Weinheim, **1993**.

[3] P. Belser, S. Bernhard, C. Blum, A. Beyeler, L. De Cola, V. Balzani, *Coord. Chem. Rev.* **1999**, *192*, 155.

[4] a) F. Diederich, C. Thilgen, *Science* **1996**, *271*, 317; b) M. Prato, M. Maggini, *Acc. Chem. Res.* **1998**, *31*, 519; c) *Fullerenes and Related Structures* (Ed.: A. Hirsch), *Top. Curr. Chem. Vol. 199*, Springer, Berlin, **1999**; d) *Fullerenes: Chemistry, Physics and Technology* (Ed. K. Kadish), Wiley, **2000**.

  0947-6539/01/0708-1604 $ 17.50+.50/0

[5] a) D. M. Guldi, *Chem. Commun.* **2000**, 321; b) L. Echegoyen, L. E. Echegoyen, *Acc. Chem. Res.* **1998**, *31*, 593; c) C. A. Reed, R. D. Bolskar, *Chem. Rev.* **2000**, *100*, 1075.
[6] a) M. Prato, *J. Mater. Chem.* **1997**, *7*, 1097; b) H. Imahori, Y. Sakata, *Adv. Mater.* **1997**, *9*, 537; c) N. Martín, L. Sànchez, B. Llescas, I. Pérez, *Chem. Rev.* **1998**, *98*, 2527; d) H. Imahori, Y. Sakata, *Eur. J. Org. Chem.* **1999**, 2445; e) F. Diederich, M. Gomez-Lopez, *Chem. Soc. Rev.* **1999**, *28*, 263.
[7] a) A. Juris, V. Balzani, F. Barigelletti, S. Campagna, P. Belser, A. von Zelewsky, *Coord. Chem. Rev.* **1988**, *84*, 85; b) J. P. Collin, S. Guillerez, J. P. Sauvage, F. Barigelletti, L. Flamigni, L. De Cola, V. Balzani, *Coord. Chem. Rev.* **1991**, *111*, 291; c) *Supramolecular Photochemistry* (Eds.: V. Balzani, F. Scandola), Horwood, Chichester, **1991**; d) V. Balzani, A. Juris, M. Venturi, S. Campagna, S. Serroni, *Chem. Rev.* **1996**, *96*, 759; e) M. D. Ward, *Int. J. Photoen.* **1999**, *1*, 1.
[8] M. Maggini, G. Scorrano, M. Prato, *J. Am. Chem. Soc.* **1993**, *115*, 9798.
[9] P. Ceroni, F. Paolucci, C. Paradisi, A. Juris, S. Roffia, S. Serroni, S. Campagna, A. J. Bard, *J. Am. Chem. Soc.* **1998**, *120*, 5480 and references therein.
[10] M. Marcaccio, F. Paolucci, C. Paradisi, S. Roffia, C. Fontanesi, L. J. Yellowlees, S. Serroni, S. Campagna, G. Denti, V. Balzani, *J. Am. Chem. Soc*. **1999**, *121*, 10081, and references therein.
[11] The driving force for the photoinduced ET process was calculated in the two media, according to the formula $-\Delta G_{ET} = E_{00} - e[E_{1/2}(Ru^{II}/Ru^{III}) - E_{1/2}(C_{60}/C_{60}^{-})] - \Delta G_s$, where $E_{1/2}(Ru^{II}/Ru^{III})$ and $E_{1/2}(C_{60}/C_{60}^{-})$ are the standard potentials for the Ru-centered oxidation (1.52 V) and FP-centered reduction (−0.41 V) in CH_3CN for dyad **5**. $E_{0\text{-}0}$ is the energy of the MLCT excited state of **5** (1.75 eV; from emission maximum), while ΔG_s represents the correction to the charge-separate state energy due to ion–ion and ion–solvent electrostatic interactions. This term was calculated for the two solvents within the dielectric continuum model which accounts for two spherical ions with radii r_A (FP) and r_D (dinuclear Ru complex) separated by a distance r_{DA} and immersed in a dielectric continuum with relative permittivity ε ($\varepsilon_{acetonitrile} = 35.94$, $\varepsilon_{dichloromethane} = 8.93$). $r_A = 4.4$ Å, $r_D = 9.0$ Å, and $r_{DA} = 24.9$ Å, based on a edge-to-edge distance C_{60}-dpq of 11.5 Å (r_D, and the edge-to-edge distance C_{60}-dpq have been obtained using semiempirical PM3 calculations). For CH_2Cl_2, a correction of the redox potentials obtained in CH_3CN, was performed as described in the literature: a) A. Z. Weller, *Phys. Chem*. **1982**, *93*, 1982; b) H. Imahori, K. Hagiwara, M. Aoki, T. Akiyama, S. Taniguchi, T. Okada, M. Shirakawa, Y. Sakata, *J. Am. Chem. Soc.*, **1996**, *118*, 11771; c) S. I. Van Dijk, C. P. Groen, F. Hartl, A. Brouwer, J. W. Verhoeven, *J. Am. Chem. Soc.*, **1996**, *118*, 8425.
[12] a) N. H. Damrauer, J. K. McCusker *J. Phys. Chem. A* **1999**, *103*, 8440; b) N. H. Damrauer, G. Cerullo, A. Yeh, T. R. Boussie, C. V. Shank, J. K. McCusker *Science* **1997**, *275*, 54.
[13] For pulse radiolytically oxidation of ruthenium complexes see: a) Q. G. Mulazzani, M. Venturi, F. Bolletta, V. Balzani, *Inorg. Chim. Acta* **1986**, *113*, L1; b) S. Das, P. V. Kamat, *J. Phys. Chem. B* **1998**, *102*, 8954.
[14] For pulse radiolytic reduction of fullerenes see: a) D. M. Guldi, H. Hungerbühler, E. Janata, K.-D. Asmus, *J. Phys. Chem.* **1993**, *97*, 11258; b) D. M. Guldi, *J. Phys. Chem. B* **2000**, *104*, 1483.
[15] a) C. S. Foote, *Top. Curr. Chem.* **1994**, *169*, 347; b) Y.-P. Sun in *Molecular and Supramolecular Photochemistry, Vol. 1* (Eds.: V. Ramamurthy, K. S. Schanze), Marcel Dekker, New York, **1997**, p. 325.
[16] a) J. L. Segura, R. Gómez, N. Martín, C. Luo, D. M. Guldi, *Chem. Commun.* **2000**, 701; b) N. Armaroli, F. Barigelletti, P. Ceroni, J.-F. Eckert, J.-F. Nicoud, J.-F. Nierengarten, *Chem. Commun.* **2000**, 599; c) I. B. Martini, B. Ma, T. Da Ros, R. Helgeson, F. Wudl, B. J. Schwartz *Chem. Phys. Lett.* **2000**, *327*, 253.
[17] C. Luo, D. M. Guldi, M. Maggini, E. Menna, S. Mondini, N. A. Kotov, M. Prato, *Angew. Chem.* **2000**, *112*, 4052; *Angew. Chem. Int. Ed.* **2000**, *39*, 3905.
[18] A. Bianco, F. Gasparrini, M. Maggini, D. Misiti, A. Polese, M. Prato, G. Scorrano, C. Toniolo, C. Villani, *J. Am. Chem. Soc.* **1997**, *119*, 7550.
[19] Thomas, M. D.; Hug, G. L. *Computers Chem.* **1998**, *22*, 491.
[20] G. L. Hug, Y. Wang, C. Schöneich, P.-Y. Jiang, R. W. Fessenden, *Rad. Phys. Chem* **1999**, *54*, 559.
[21] P. Belser, A. von Zelewsky, *Helv. Chim. Acta* **1980**, *63*, 1675.
[22] M. Carano, P. Ceroni, L. Mottier, F. Paolucci, S. Roffia, *J. Electrochem. Soc.* **1999**, *146*, 3357.

Received: May 22, 2000
Revised: November 8, 2000 [F2504]